ChemComm

COMMUNICATION

View Article Online
View Journal | View Issue

Cite this: *Chem. Commun.*, 2015, **51**, 569

Received 23rd September 2014,
Accepted 11th November 2014

DOI: 10.1039/c4cc07518h

www.rsc.org/chemcomm

Efficient photovoltaic and electroluminescent perovskite devices†

Lidón Gil-Escrig,‡ Giulia Longo,‡ Antonio Pertegás, Cristina Roldán-Carmona, A. Soriano, Michele Sessolo and Henk J. Bolink*

Planar diode structures employing hybrid organic–inorganic methylammonium lead iodide perovskites lead to multifunctional devices exhibiting both a high photovoltaic efficiency and good electroluminescence. The electroluminescence strongly improves at higher current density applied using a pulsed driving method.

Hybrid organic–inorganic methylammonium lead iodide perovskites ($CH_3NH_3PbI_3$) have recently been used to prepare very efficient solar cells.[1–11] Previously, these materials have been used to prepare light-emitting diodes (LEDs).[12,13] Electroluminescence was first shown at very low temperatures,[14] and later by incorporating an organic emitter also at room temperature.[12] These devices, however, were not obtained with the same material used in recent efficient solar cells, *i.e.* the methylammonium lead iodide which adopts the 3D perovskite structure. The LEDs were fabricated using 2D layered lead iodide and chloride perovskites containing longer alkylammonium salts. Recently, it was demonstrated that also the 3D $CH_3NH_3PbI_3$ perovskite exhibits strong photoluminescence quantum yield (PLQY) up to 70% at high excitation intensity,[15] and were incorporated into LEDs.[16] Hence, this opens up the possibility to prepare a multi-functional device that shows simultaneously efficient photocurrent generation and electroluminescence.[17] Such devices were shown previously, albeit with rather low photovoltaic efficiency (<1%).[18–20]

Two main types of architectures for $CH_3NH_3PbI_3$ based photovoltaic devices have been demonstrated so far, either using mesoporous metal oxide scaffolds or planar structures.[3,4,21] In the latter either a metal oxide or an organic hole blocking layer is employed, resulting in the transparent bottom electrode being the electron or hole collector, respectively. Recently, we showed a device architecture in which the perovskite layer is sandwiched in between an organic hole and electron blocking layer leading to photovoltaic efficiencies close to 15%.[5,22] Such a structure is frequently used in organic light-emitting diodes (OLEDs) to confine electrons and holes in the light-emitting layer.[23] In a similar device layout and using $CH_3NH_3PbBr_3$ perovskite nanoparticles bright green electroluminescence was observed.[24] Thin films based on these perovskite nanoparticles exhibited PLQY's above 20% at low excitation intensity. Therefore, the planar architecture with the hole and electron blocking layers is also expected to lead to efficient light-emission in view of the high PLQY's observed in thin films of $CH_3NH_3PbI_3$. However, a high work function electrode, Au, was used in the solar cell configuration. Even though it works well to extract electrons, it is not ideal for their injection into to the lowest unoccupied molecular orbital (LUMO) of the electron transporting layer. Therefore, we have adapted the architecture by employing a thicker electron transporting–hole blocking layer and a low workfunction top electrode. Using this architecture the device exhibits simultaneously a high photovoltaic efficiency and good electroluminescence.

The device layout is shown in Fig. 1a and consists of a 80 nm poly(3,4-ethylenedioxythiophene):poly(styrene sulfonic acid) (PEDOT:PSS) layer and a thin layer (20 nm) of poly[*N*,*N*′-bis(4-butylphenyl)-*N*,*N*′-bis(phenyl)benzidine] (polyTPD) as the electron blocking layer. On top of this, the $CH_3NH_3PbI_3$ was thermally evaporated to a thickness of 320 nm, using a protocol described previously,[5] followed by a hole blocking layer of [6,6]-phenyl C_{61}-butyric acid methylester (PCBM) (100 nm).[25] The device was

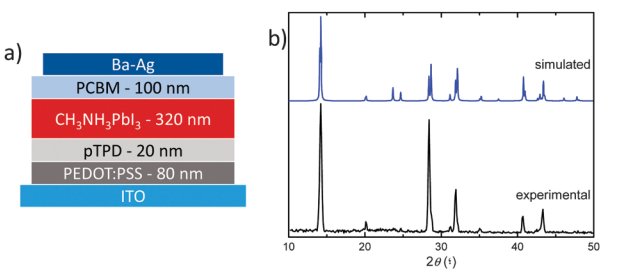

Fig. 1 (a) Device layout. (b) Simulated and experimental grazing incidence X-ray diffraction (GIXRD) pattern for a $CH_3NH_3PbI_3$ perovskite thin film.

Instituto de Ciencia Molecular, Universidad de Valencia, c/Catedrático J. Beltrán, 2, 46980 Paterna, Spain. E-mail: henk.bolink@uv.es

† Electronic supplementary information (ESI) available: Distribution of the power conversion efficiencies and EQE_{EL} for a series of devices, EQE *vs.* current density and materials and methods. See DOI: 10.1039/c4cc07518h

‡ These authors contributed equally to this work.

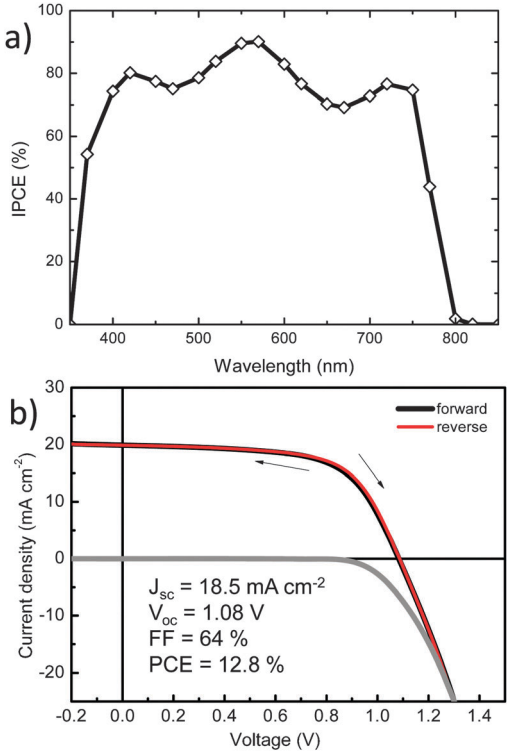

Fig. 2 (a) Typical IPCE spectrum for the solar cells. (b) *J–V* curves in the dark (gray line) and under 1 sun illumination using forward and reverse scan directions (black and red line, respectively).

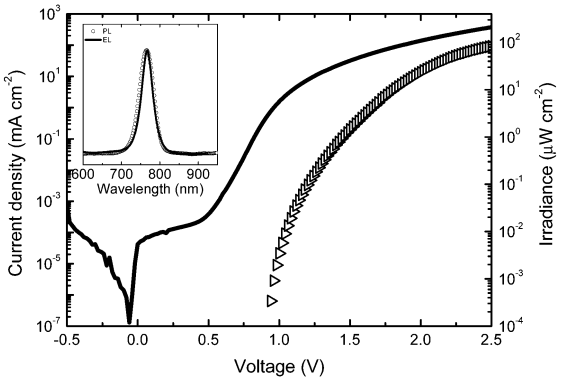

Fig. 3 Current density (line) and radiance (open triangles) *versus* applied voltage. Inset: electroluminescence (EL) spectrum (solid line) emitted by the device and photoluminescence (PL) spectrum (open circles) recorded using a 405 nm CW laser as the excitation source.

completed by the evaporation of a Ba (10 nm) top electrode covered with Ag (100 nm). Both the polyTPD and the PCBM layers were deposited using a meniscus coating process to ensure high quality films.[26] The X-ray diffraction pattern of the $CH_3NH_3PbI_3$ layer is shown in Fig. 1b demonstrating a good match with the calculated one and ensuring the formation of the perovskite structure.

First, the photovoltaic effect of these devices was examined. The incident photon to electron conversion efficiency (IPCE, Fig. 2a) was determined as a function of wavelength and the current density *versus* voltage characteristics (*J–V*, Fig. 2b) were determined in dark and under 1 sun illumination. The key performance data are similar to those obtained previously for similar devices yet with an Au top (electron collecting) electrode.[5,22] The spread of performances for a series of devices is depicted in Fig. S1 (ESI†).

In the next step we used this same device configuration and evaluated the radiative recombination (emission) and the current density *versus* applied voltage of various devices. A sensitive Si-photodiode coupled to an integrating sphere was used to obtain the irradiance of the device. The emission spectrum is shown in Fig. 3, with a maximum at 765 nm. The irradiance rapidly increases around an applied voltage of 0.9 V and reaches values of 84 μW cm^{-2} at 2.5 V (Fig. 3). The low voltage required for electroluminescence is indicative of very good charge transport properties in this device stack. The *J–V* curves (Fig. 3) shows the typical diode characteristics with a sharp current rise related to the diffusion current. A flat-band or build-in potential (V_{bi}) of 1 V was estimated with the deviation from the diffusion limited regime.[27]

This implies that the open circuit voltage V_{oc} is slightly above the V_{bi}. Yet, the S-shape curve which is frequently observed in such cases for organic photovoltaic devices, is here not seen.[28] Apparently, in these perovskite devices the diffusion current is sufficiently high.

The external quantum efficiency (EQE_{EL}) of the device reaches a maximum of approximately 0.04% (Fig. S2, ESI†). This is similar to the EQE_{EL} previously reported by us for the devices using a gold top electrode (0.012%).[29] The spread of performances of the EQE_{EL} for different devices is shown in Fig. S3 (ESI†). Such efficiencies are approximately 2 orders of magnitude lower than the most efficient thin film near infrared emitting devices.[30,31] The PLQY of a similar perovskite material, the so-called mixed halogen perovskites $CH_3NH_3PbI_{3-x}Cl_x$, is strongly dependent on the excitation intensity in the range from 25 to 2000 mW cm^{-2}.[15] In our devices the $CH_3NH_3PbI_3$ is prepared from only the iodide precursors and we were unable to detect a photoluminescence signal using a quantum yield measurement system (C9920-02, Hamamatsu Photonics) with a Xe lamp as the excitation source and a multichannel spectrometer (Hamamatsu PMA-11) as the optical detector. Using the same setup for a film containing $CH_3NH_3PbBr_3$ perovskite nanoparticles we observed a PLQY of 23%.[24] Only when the $CH_3NH_3PbI_3$ is excited with a CW laser (at 405 nm) a photoluminescence signal could be observed.[29] In the multifunctional device employing $CH_3NH_3PbI_3$ the electroluminescence increases with increasing current density (Fig. 4a). Holes and electrons are confined to the perovskite layer due to the efficient electron and hole blocking materials adjacent to it. This therefore leads to a strong increase in excitons formation and thus electroluminescence in that layer. Hence, a similar behavior as was observed for the $CH_3NH_3PbI_{3-x}Cl_x$ perovskite might take place. In order to increase the excitation intensity, the devices were driven with pulsed current using a periodic square waveform, with duty cycle of 50% at a frequency of 100 Hz. This allows for much higher current densities while avoiding rapid degradation as the device is allowed to relax (dissipate excess heat) in the off state. Average current densities up to 1150 mA cm^{-2} (Fig. 4a), corresponding to 2300 mA cm^{-2} in the on phase of the pulse (Fig. 4b), were obtained. The resulting irradiance increases steadily,

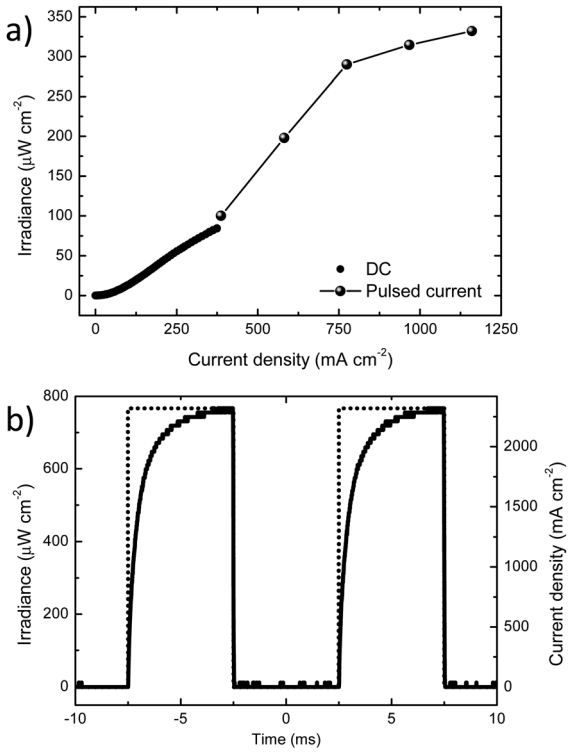

Fig. 4 (a) Irradiance *versus* current density for a dc- (symbols) and a pulsed current-driven (line and symbols) device. Two regimes define the different operation modes: up to a current density of 375 mA cm^{-2} the device was operated in dc mode, beyond that the current was applied as a square waveform, with a duty cycle of 50% at a frequency of 100 Hz. (b) Detail of the irradiance when the device is operated in the pulsed current mode.

exceeding 330 μW cm^{-2} at the maximum current density. The radiance meter integrates the emitted photons over a period of 100 ms and as such records the average emission. Hence, the light output was also measured using a Si-photodiode coupled to an oscilloscope enabling the visualization of the on–off cycles in correspondence to the applied current pulses (Fig. 4b). Intense electroluminescence up to 770 μW cm^{-2} is reached in the pulse peak with a rising time (time to reach 90% of the maximum signal) of approximately 4 ms. This slow response can be ascribed either to a low exciton formation rate or to a slow depletion of the exciton quenching sites, or both.

In summary, a simple thin film device consisting of a hybrid organic–inorganic perovskite as the absorbing and emitting layer, sandwiched in between organic electron and hole blocking layers, can be used to efficiently generate electricity and light depending on the operation conditions. The photovoltaic power conversion efficiency of 12.8% is among the highest recorded for similar thin film devices. The electroluminescence observed when driving the device in pulsed current mode reaches interesting values and the external quantum yield is only two orders of magnitude below the best performing near infrared planar LED. This is remarkable in view of the very low PLQY of the active material used, and implies a prospect towards applications for these devices when strategies are employed to increase the PLQY.

We acknowledge Dr Kristofer Tvingstedt from the Julius Maximilians University of Würzburg for the CW laser excited PL measurements and Jorge Ferrando for the pulsed EL measurements. This work has been supported by the European Union 7th framework program LUMINET (grant 316906), the Spanish Ministry of Economy and Competitiveness (MINECO) (MAT2011-24594) and the Generalitat Valenciana (Prometeo/2012/053). A.P. acknowledges MINECO for an FPI grant.

Notes and references

1 M. M. Lee, J. Teuscher, T. Miyasaka, T. N. Murakami and H. J. Snaith, *Science*, 2012, **338**, 643–647.
2 J. M. Ball, M. M. Lee, A. Hey and H. J. Snaith, *Energy Environ. Sci.*, 2013, **6**, 1739–1743.
3 J. Burschka, N. Pellet, S.-J. Moon, R. Humphry-Baker, P. Gao, M. K. Nazeeruddin and M. Gratzel, *Nature*, 2013, **499**, 316–319.
4 M. Liu, M. B. Johnston and H. J. Snaith, *Nature*, 2013, **501**, 395–398.
5 O. Malinkiewicz, A. Yella, Y. H. Lee, G. M. Espallargas, M. Graetzel, M. K. Nazeeruddin and H. J. Bolink, *Nat. Photonics*, 2014, **8**, 128–132.
6 D. Liu and T. L. Kelly, *Nat. Photonics*, 2014, **8**, 133–138.
7 N. J. Jeon, H. G. Lee, Y. C. Kim, J. Seo, J. H. Noh, J. Lee and S. I. Seok, *J. Am. Chem. Soc.*, 2014, **136**, 7837–7840.
8 Q. Chen, H. P. Zhou, Z. R. Hong, S. Luo, H. S. Duan, H. H. Wang, Y. S. Liu, G. Li and Y. Yang, *J. Am. Chem. Soc.*, 2014, **136**, 622–625.
9 H. S. Kim, J. W. Lee, N. Yantara, P. P. Boix, S. A. Kulkarni, S. Mhaisalkar, M. Gratzel and N. G. Park, *Nano Lett.*, 2013, **13**, 2412–2417.
10 W.-J. Yin, T. Shi and Y. Yan, *Adv. Mater.*, 2014, **26**, 4653–4658.
11 M. A. Green, A. Ho-Baillie and H. J. Snaith, *Nat. Photonics*, 2014, **8**, 506–514.
12 K. Chondroudis and D. B. Mitzi, *Chem. Mater.*, 1999, **11**, 3028–3030.
13 T. Hattori, T. Taira, M. Era, T. Tsutsui and S. Saito, *Chem. Phys. Lett.*, 1996, **254**, 103–108.
14 M. Era, S. Morimoto, T. Tsutsui and S. Saito, *Appl. Phys. Lett.*, 1994, **65**, 676.
15 F. Deschler, M. Price, S. Pathak, L. E. Klintberg, D.-D. Jarausch, R. Higler, S. Hüttner, T. Leijtens, S. D. Stranks, H. J. Snaith, M. Atatüre, R. T. Phillips and R. H. Friend, *J. Phys. Chem. Lett.*, 2014, **5**, 1421–1426.
16 Z.-K. Tan, R. S. Moghaddam, M. L. Lai, P. Docampo, R. Higler, F. Deschler, M. Price, A. Sadhanala, L. M. Pazos, D. Credgington, F. Hanusch, T. Bein, H. J. Snaith and R. H. Friend, *Nat. Nanotechnol.*, 2014, **9**, 687–692.
17 A. K. Pandey and J. M. Nunzi, *Adv. Mater.*, 2007, **19**, 3613–3617.
18 G. Yu, C. Zhang and A. J. Heeger, *Appl. Phys. Lett.*, 1994, **64**, 1540–1542.
19 W. Rieβ, S. Karg, V. Dyakonov, M. Meier and M. Schwoerer, *J. Lumin.*, 1994, **60–61**, 906–911.
20 D. A. Bernards, S. Flores-Torres, H. D. Abruña and G. G. Malliaras, *Science*, 2006, **313**, 1416–1419.
21 H. J. Snaith, *J. Phys. Chem. Lett.*, 2013, **4**, 3623–3630.
22 O. Malinkiewicz, C. Roldán-Carmona, A. Soriano, E. Bandiello, L. Camacho, M. K. Nazeeruddin and H. J. Bolink, *Adv. Energy Mater.*, 2014, 1400345.
23 H. Sasabe and J. Kido, *J. Mater. Chem. C*, 2013, **1**, 1699–1707.
24 L. C. Schmidt, A. Pertegas, S. Gonzalez-Carrero, O. Malinkiewicz, S. Agouram, G. Minguez Espallargas, H. J. Bolink, R. E. Galian and J. Perez-Prieto, *J. Am. Chem. Soc.*, 2014, **136**, 850–853.
25 G. Yu, J. Gao, J. C. Hummelen, F. Wudl and A. J. Heeger, *Science*, 1995, **270**, 1789–1791.
26 O. Malinkiewicz, M. Lenes, H. Brine and H. J. Bolink, *RSC Adv.*, 2012, **2**, 3335–3339.
27 P. de Bruyn, A. H. P. van Rest, G. A. H. Wetzelaer, D. M. de Leeuw and P. W. M. Blom, *Phys. Rev. Lett.*, 2013, **111**, 186801.
28 C. Uhrich, D. Wynands, S. Olthof, M. K. Riede, K. Leo, S. Sonntag, B. Maennig and M. Pfeiffer, *J. Appl. Phys.*, 2008, **104**, 043107.
29 K. Tvingstedt, O. Malinkiewicz, A. Baumann, C. Deibel, H. J. Snaith, V. Dyakonov and H. J. Bolink, *Sci. Rep.*, 2014, **4**, 6071.
30 C. Borek, K. Hanson, P. I. Djurovich, M. E. Thompson, K. Aznavour, R. Bau, Y. R. Sun, S. R. Forrest, J. Brooks, L. Michalski and J. Brown, *Angew. Chem., Int. Ed.*, 2007, **46**, 1109–1112.
31 A. Pertegas, N. M. Shavaleev, D. Tordera, E. Orti, M. K. Nazeeruddin and H. J. Bolink, *J. Mater. Chem. C*, 2014, **2**, 1605–1611.